Break-up of Pt catalyst surfaces by high CO coverage

Feng Tao,[1,2] Sefa Dag,[3] Lin-Wang Wang,[3] Zhi Liu, [4] Derek R. Butcher,[1,2] Hendrik Bluhm,[5] Miquel Salmeron,[2]* Gabor A. Somorjai [1,2]*

Materials Science Division, Lawrence Berkeley National Lab, Berkeley CA 94720 [1]
Department of Chemistry, University of California, Berkeley CA 94720 [2]
National Energy Research Scientific Computing Center, Lawrence Berkeley National Lab, Berkeley CA 94720 [3]
Advanced Light Source, Lawrence Berkeley National Lab, Berkeley CA 94720 [4]
Chemical Science Division, Lawrence Berkeley National Lab, Berkeley CA 94720[5]

Stepped Platinum surfaces were found to undergo extensive and reversible restructuring when exposed to CO at pressures above 0.1 Torr. This radically new and previously unknown restructuring phenomenon, has important implications for Pt based catalytic reactions. Novel Scanning Tunneling Microscopy and Photoelectron Spectroscopy techniques operating under gaseous environments near ambient pressure and temperature revealed that as the CO surface coverage approaches 100%, the originally flat terraces of stepped Pt crystals break up into nanometer size clusters. At room temperature the crystal surface reverts to its initial flat morphology after pumping away the gas phase CO. Density Functional Theory energy calculations provide a rationale for the observations whereby the creation of increased concentrations of low coordination Pt sites at the edges of the formed nanoclusters relieves the strong CO-CO repulsion in the highly compressed adsorbate film.

* Corresponding authors. Email: somorjai@berkeley.edu; mbsalmeron@lbl.gov

Industrial catalysts usually consist of small particles exposing different atomic terminations that exhibit a high concentration of step, kink sites, and vacancies at the edge of the facets, which are thought to be the catalytically active sites (*1-3*). Stepped single crystal surfaces with well-defined structures can be prepared with a high density of such sites. They are the most promising models of the real catalysts since such vicinal surfaces mimic more closely the rough regions of industrial catalyst surfaces, which can be critical for their catalytic properties.

The structure of a surface however is not static and can change from that of the clean crystal when adsorbates are bound to it, a phenomenon well known in surface science (1-2). However, past surface science experiments were usually performed in high vacuum conditions where the high adsorbate coverage characteristic of industrial catalysts cannot be usually attained, unless the samples are kept at low temperature. This is likely to inhibit any restructuring that requires overcoming of even moderate activation barriers. Real catalysts on the other hand operate under pressures ranging from milliTorr to atmospheres and at room temperature at or above room temperature, so that the surfaces can easily change and adopt the structure corresponding to thermodynamic equilibrium. We overcame the limitations of traditional surface science techniques using new tools developed in our laboratories, including high-pressure scanning tunneling microscopy (STM), and ambient pressure photoelectron spectroscopy (AP-XPS) (*4-8*) (Figs. S1 and S2). With these techniques we were able to image the atomic structure and identify the chemical state of catalyst atoms and adsorbed reactant molecules under realistic conditions. Here we concentrate on carbon monoxide, one of the most common reactants of numerous important industrial catalytic processes such as Fischer-Tropsch

synthesis (*9,10*), CO oxidation in automobile catalytic converters (*11*), and degradation of Pt electrodes in hydrogen fuel cells (*12-14*).

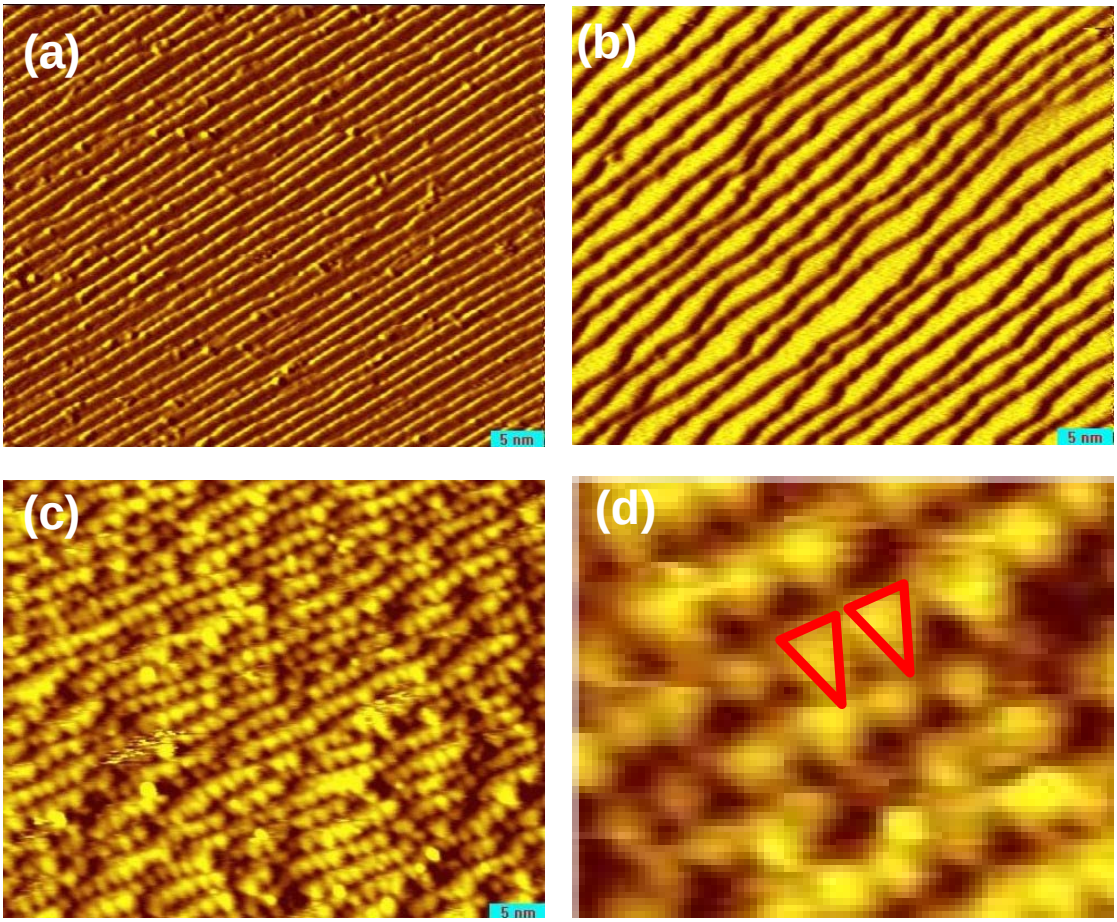

Fig. 1. STM images of clean Pt(557): (a) in ultra-high vacuum UHV with a background pressure of 1×10^{-10} Torr; (b) under ~5×10^{-8} Torr of CO; (c) under 1 Torr of CO. All the three STM images are 40 nm × 50 nm in size. (d) Enlarged view of Fig. 1(c) showing the roughly triangular shape of the nanoclusters formed at 1 Torr. Two of the triangular nanoclusters are marked with red lines.

Our studies revealed an unexpected and reversible large scale restructuring of the surfaces of two Pt stepped surfaces, Pt(557) and Pt(332), both consisting of six atoms wide terraces of (111) orientation separated by monoatomic steps with different orientations. On Pt(557) the step atoms form a (100)-type square cell, while on Pt(332) they form a (111)-type triangular cell (Fig. S3). Under high coverage of CO we observed

the break-up of the originally flat terraces into an array of nanoclusters aligned along the step directions. Density Functional Theory (DFT) calculations were performed to help understand the energetics and the mechanisms underlying the restructuring from steps and flat terraces to nanoclusters.

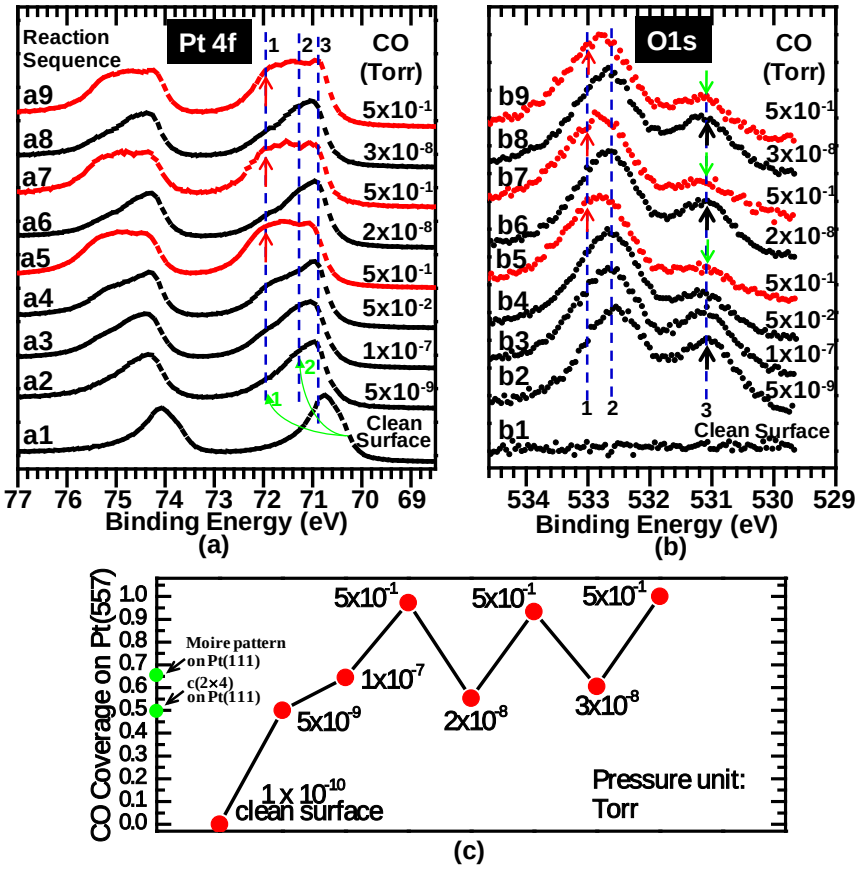

Fig. 2. Photoemission spectra of Pt4f (a) and O1s (b) under different reaction conditions. The red spectra were obtained at a CO pressure of 5×10^{-1} Torr. Binding energies were referenced to the Fermi level. The red arrows in (a) show the increase in photoemission intensity in the high binding energy side of $Pt4f_{7/2}$. The green arrows 1 and 2 in (a) mark significant chemical shifts upon chemisorptions. The red and green arrows in (b) mark the increase of photoemission intensity in the high binding energy side of the O1s spectra and the simultaneous decrease in the low binding energy side at high pressure, respectively. The dark arrows in (b) mark the relatively larger ratios of photoemission intensity at low binding energy side at low pressure, compared to the ratios at high pressure. (c) Coverage of CO molecules on Pt(557) under different CO pressures determined from the XPS peak areas calibrated using the published 0.5 coverage of CO in the low pressure c(2×4) structure; the green dots on the left Y-axis mark the coverage of CO of c(2×4) structure on Pt(111) formed at low pressure 5×10^{-9} Torr (*16,17*), and the coverage of CO of moire pattern formed on Pt(111) at 1 Torr of CO (*18*).

Fig.1 shows representative images of the Pt(557) under UHV conditions (base pressure 1×10^{-10} Torr), under ~10^{-7} Torr of CO, and under 1 Torr of CO. When CO was introduced in the reactor cell at low pressure the initially straight steps become wavy (Fig. 1b). The STM images also revealed a doubling of terrace width and step height on the Pt(557) surface (Fig. S4b2 and Fig.S5b). Interestingly, on Pt(332) the step edges did not increase their roughness under the same pressure conditions, a result that we ascribe to the different atomic packing of the Pt(332) and Pt(557) steps (Fig. S3c and S3d). More dramatic effects occur when the CO pressure is increased to 0.1 Torr and higher. The terraces on Pt(557) break down into nanoclusters about 2.2 nm × 2.1 nm in size, along [112] and [1-10] directions (Fig. 1c). Interestingly, the nanoclusters have a roughly triangular shape with the vertex pointing into the lower terrace. On Pt(332) the nanoclusters are rectangular or roughly parallelogram shaped (Fig. S6b), a difference in geometry that is probably related to the different step geometries and electronic structures there. Line profiles (Fig. S4d2) indicate that on Pt(557) the nanoclusters in adjacent terraces are separated by 4.4 Å, i.e., two atoms in height; neighboring nanoclusters in the same terrace being separated by approximately 2 Å deep gaps, i.e., a single-atom.

XPS experiments under similar pressure conditions (Figs. 2a, 2b, and S7) reveal several peaks from the Pt4f core level corresponding to atoms in different coordination geometries (bulk, surface, and under-coordinated sites), and O1s peaks from CO bound to different sites (top, bridge, and under-coordinated sites). The deconvoluted Pt4f spectra (Fig. S7) show the significant increase of the relative intensity of the peak around ~72.15 eV, which we attribute to under-coordinated Pt atoms at step edges or/and cluster peripheries for pressures of 0.1 Torr or higher. In the oxygen region (Fig. 2b), two

photoemission peaks (Fig. 2b2) are observed that indicates two major adsorption sites on the terraces at low pressure (<5 $\times 10^{-2}$ Torr), consistent with the O1s photoemission features at ~532.7 and ~531.1 eV for CO bonded to on-top and bridge sites on Pt(111), respectively (*15, 16*). A third peak at ~533.1 eV at a pressure higher than 5 $\times 10^{-2}$ Torr is attributed to CO bound to under-coordinated Pt atoms. With increasing CO coverage there is a decrease of relative intensity of the O 1s peak at ~532.6 (on-top sites) and ~531.0 (bridge sites) and an increase of that at 533.1 eV (under-coordinated sites) as the CO pressure increased to 5×10^{-1}. At 5×10^{-1} Torr the peak at ~533.1 eV is the largest (Fig. S7, *b4*, *b6*, and *b8*). The reversible changes of the Pt4f and O1s photoemission features as the CO pressure changes from high (5×10^{-1} Torr) to low (2×10^{-8} or 3×10^{-8} Torr) (Fig. 2), suggest that the morphological changes in the surface structure are also reversible. This is indeed supported by the observed reversible formation and disappearance of nanoclusters as the pressure is cycled between high and low, as shown in Fig. S8. A similar reversible formation of nanoclusters at high pressure was observed on Pt(332).

XPS allows us to determine the coverage of CO as a function of pressure as shown in Fig. 2c. On Pt(557) the high pressure coverage is 1.94 times that at low pressure (5×10^{-9} Torr). Using the known coverage of 0.5 for CO in the c(2×4) adsorption layer on Pt(322), Pt(355) and Pt(111) (*17-19*), at 5×10^{-9} Torr at room temperature to calibrate the XPS peak areas, the coverage of CO on Pt(557) is ~0.97 at 5×10^{-1} Torr. The coverage decreased to ~0.5 after pumping out the CO, and increased again to ~0.93 after reintroducing CO at 5×10^{-1} Torr. Similarly, the CO coverage on Pt(332) at high pressure is 0.3-0.4 higher than that at low pressure (10^{-9} - 10^{-7} Torr), and it alternately increases and decreases at high pressure and low pressure (Figs. S10 and S11). Such dramatic

changes in real space structure, shown by STM, and core level binding energies, shown by XPS, between high pressure and low pressure on Pt(557) and Pt(332) were not observed on Pt(111) by XPS (Fig. S9) and STM under the same conditions (19).

The reason for the observed changes must be related to the very high coverage of CO, one molecule per surface Pt atom, which cannot be achieved under vacuum. This high density should result in a strong repulsion between CO molecules. We thus propose that the restructuring of the surface is driven by the relaxation of the repulsive CO-CO interaction facilitated by the formation of nanoclusters. Such restructuring provides a substantial increase in the number of edge atoms which have low coordination number and where CO molecules can tilt away from the center and thus decrease their mutual repulsion. We found this broken-up surface is active for CO oxidation even at room temperature[20], possibly due to a low activation barrier of CO molecules on such nanoclusters with 100% CO coverage.

DFT calculations were carried out to help understand this phenomenon. The calculations were done using the experimentally observed surface structure and CO coverage as starting points. In the low pressure regime ($<10^{-3}$ Torr), a c(2×4) CO adlayer with a coverage of 0.5 on the flat terraces is assumed, while at 0.1 Torr or higher a full CO layer with coverage of 1 was assumed. Calculations were carried out on a clean surface with single-atom height steps, on a surface with double terrace widths and double-atom heights, and on a surface restructured with triangular and parallelogram shaped clusters. In order to compare their energies, the chemical potentials for Pt and CO were used to account for possible difference in the number of atoms and molecules in different systems with the same surface area. While the Pt chemical potential is just the

bulk Pt binding energy, the CO chemical potential was calculated from the pressure dependent gas phase entropy (see the supplementary material). On the clean Pt(557) surface the single-atom height step structure is energetically more favorable than that with double-atom height by 0.12 eV per edge atom (Table S1). The double-width terrace structure is energetically more favorable by 0.40 eV per edge atom upon adsorption of CO in a c(2×4) layer, consistent with the experimental observations (Fig.1(a) to Fig.1(b)). In contrast to Pt(557), calculations show that on Pt(332) the surface with double-atom step heights is not more thermodynamically stable upon CO adsorption (Table S1), again in agreement with the experimental results.

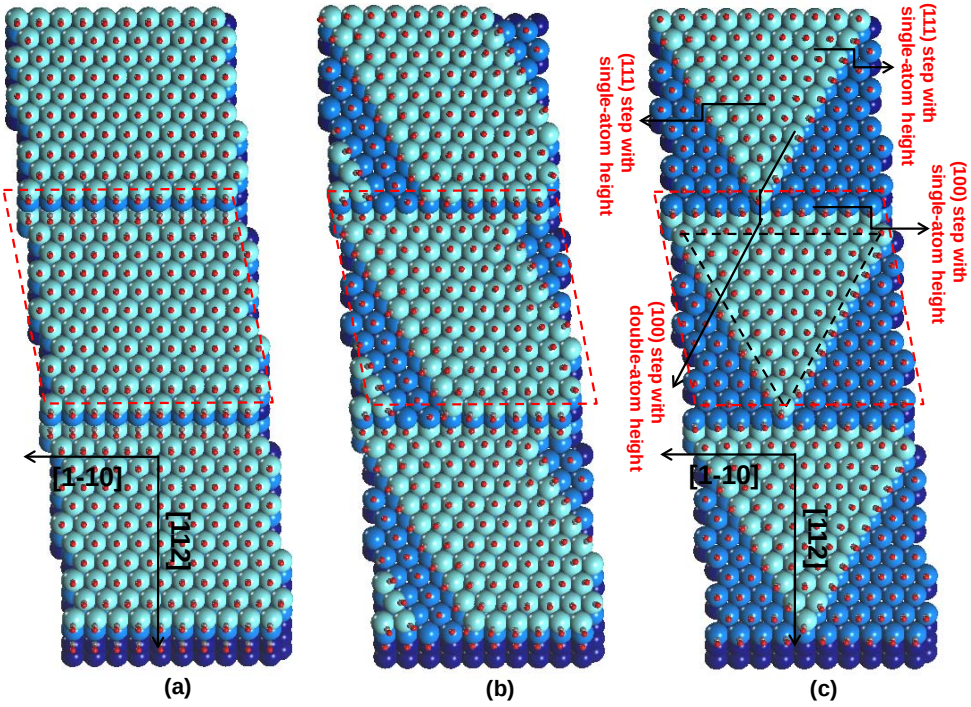

Fig. 3. Models of the double-stepped Pt(557) surface covered by CO at high pressure used in the DFT calculations: (a) unrestructured terrace, (b) parallelogram shaped nanoclusters, and (c) triangular shaped nanoclusters. Red dash frames in each picture show the periodic supercell. First and second layer Pt atoms are represented with light green and blue balls, respectively. Red dots represent CO molecules.

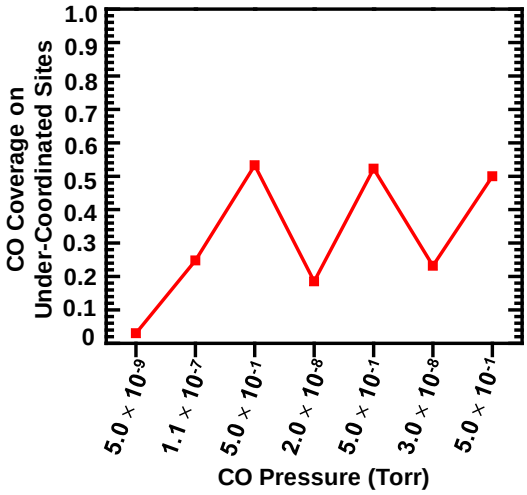

Fig. 4. Evolution of the fractions of CO molecules adsorbed on bridge, atop, and under-coordinated sites as a function of pressure.

For the high pressure (1×1) CO layer on Pt(557) we calculated the total free energy for clusters of different shapes on the double terraces. Three cases were calculated and compared, as shown in Fig. 3: a flat double terrace (a), a parallelogram created by removing two rows of Pt atoms (b), and a triangle nanocluster crossing the width of a terrace (c). For the double terrace (Fig. S5b), whether CO molecules are adsorbed on Pt atoms at the step-bottom side (A1 in Fig. S5b) or not gives a slightly different total energy of the slab. The calculation shows that covering the step-down side will reduce the total free energy by 0.144 eV per atom. This energy difference is much smaller than the adsorption energy of CO on the nanoclusters. Thus, as shown in Fig. 3, each Pt atoms in the step-down side adsorbs one CO molecule in the calculation. The total free energies of these three systems (Table S2) show that the structure with triangle shaped nanoclusters has the lowest free energy, followed by the parallelogram, and then by the flat double terrace. In the final structure after relaxation the CO molecules adsorbed at the edge of the nanoclusters fan-out significantly. This binding configuration reduces the

repulsion between adjacent CO molecules and therefore decreases the total energy. The significantly increased density of under-coordinated Pt sites and of CO molecules bound to such sites (*21a*) is consistent with the XPS photoemission features of O1s and Pt4f. For example, the coverage of CO molecules bound to under-coordinated sites of nanoclusters is ~ 55% (*21b*) at 0.1 Torr or higher (Fig. 4); however, it is ~ 20%-22% at 10^{-8}-10^{-7} Torr (Fig 4) (*21c*).

In conclusion, we have discovered the occurrence of large scale surface restructuring of stepped Pt crystals, which are model catalysts for many reactions. Thanks to *in-situ* studies using high-pressure STM and ambient-pressure XPS, and DFT calculations, we have shown the reversible break-up of the surface into nanoclusters covering surface at CO pressures characteristic of industrial reactions. This result is driven by strong repulsion between CO molecules when coverage reaches 100% and leads to a large increase in the number of under-coordinated Pt atoms decorating the nanocluster edges. It indicates an intrinsic connection between surface coverage of reactant molecules and atomic arrangement of catalyst surface under reaction conditions. These results have important implications for catalysis where high pressures and high coverages of reactant molecules on the catalyst surfaces are the norm.

References

1. G. Ertl, H. Knözinger, F. Schüth, and J. Weitkamp, *Handbook of Heterogeneous Catalysis*, VCH-Wiley, 2008.
2. G. A. Somorjai, *Introduction to Surface Chemistry and Catalysis*, VCH-Wiley, 1997.
3. C. Burda, X. Chen, R. Narayanan, M. A. El-Sayed, *Chem. Rev.* **105**, 1025 (2005).
4. http://www.er.doe.gov/bes/reports/abstracts.html#GC
5. F. Tao, D. Tang, M. Salmeron, G. A. Somorjai, *Rev. Sci. Instrum.* **79**, 084101 (2008).
6. D. F. Ogletree , H. Bluhm , G. Lebedev , C. S. Fadley , Z. Hussain , M. Salmeron, *Rev. Sci. Instrum.* **73**, 3872 (2002).
7. M.Salmeron, R. Schloegl, *Surf. Sci. Rep.* **63**, 169 (2008).
8. H. Bluhm, M. Havecker, A. Knop-Gericke, M. Kiskinova, R. Schloegl, M. *MRS Bull.* **32**, 10222 (2007).
9. J. M. Thomas, W. J. Thomas, *Principles and Practices of Heterogeneous Catalysis*, Wiley VCH, 1997, chapter 8.
10. T. Herranz, X. Deng, A. Cabot, J. Guo, and M. Salmeron. *J. Phys. Chem. B.* **113,** 10721 (2009)
11. X. W. Xie, Y. Li, Z. Q. Liu, M. Haruta, W. J. Shen, *Nature* **458**, 746 (2009).
12. J. A. Rodriguez, S. Ma, P. Liu, J. Hrbek, J. Evans, M. Perez, *Science* **318**, 1757 (2007).
13. W. B. Kim, T. Voitl, G. J. Rodriguez-Rivera, J. A. Dumesic, *Science* **305** 1280 (2004).
14. Q. Fu, H. Saltsburg, M. Flytzani-Stephanopoulos, *Science* **301**, 5635 (2003).
15. O. Bjornebolm, A. Nilsson, H. Tillorg, P. Bennich, A. Sandell, B. Hernnas, C. Puglia, N. Martensson, *Surf. Sci.* **315**, L983 (1994).
16. M. Kinne, T. Fuhrmann, C. M. Whelan, J. F. Zhu, J. Pantfo¨ rder, M. Probst, G. Held, R. Denecke, H.-P. Steinru¨ck, *J. Chem. Phys.* **117**, 10852 (2002).
17. B. Tränkenschuh, N. Fritsche, T. Fuhrmann, C. Papp, J. F. Zhu, R. Denecke, H.-P. Steinrück *J. Chem. Phys.* **124**, 074712 (2006).
18. B. Trankenschuh, C. Papp, T. Fuhrmann, R. Denecke, H.-P. Steinruck, *Surf. Sci.* **601**, 1108 (2007).
19. S. R. Longwitz, J. Schnadt, E. K. Vestergaard, R. T. Vang, E. Lægsgaard, I. Stensgaard, H. Brune, F. Besenbacher, *J. Phys. Chem. B* **108**, 14497 (2008).
20. CO_2 was clearly detected from CO oxidation on Pt(557) at room temperature by a mass spectrometer installed at the second pumping stage (Fig. S1a). In this example, Pt(557) was cleaned and completely cooled to room temperature, and then 120 mTorr CO was introduced to reactor of ambient-pressure XPS. Then, 300 mTorr O_2 was introduced in this reactor. 24 mTorr CO_2 in the reactor was detected. Under the same experimental condition, no CO_2 was produced in the reactor without Pt(557) catalyst. Following the same sample preparation and experimental conditions, there was no CO_2 formed on Pt(111).
21. (a) The coverage of CO molecules bound to Pt atoms at the edge of the triangular nanoclusters used in the DFT calculation is calculated to be ~0.5 (Fig. 3c). (b) The ratio of the area of the O1s peak component from CO molecules bound to under-coordinated Pt atoms to the total peak area of the O1s peak at a pressure of 0.5 Torr is ~0.57 and the absolute coverage of CO at this pressure is 0.97. (c) The ratio of the peak area of O1s of CO molecules bound to under-coordinated Pt atoms to the total peak area of O1s of CO molecules adsorbed at a pressure of ~10^8 -10^{-7} Torr is ~36%; CO coverage at this pressure is ~0.56; The coverage of CO molecules on under-coordinated Pt sites on Pt(557) at this low pressure range is thus ~20%.
22. The experimental work was supported by the Director, Office of Basic Energy Sciences, Materials Sciences, Geosciences, and Biosciences Division. The theoretical work was supported by the Office of Advanced Scientific Computing Research. U.S. Department of Energy under Contract No. DE-AC02-05CH11231.

Supporting Online Material
www.sciencemag.org
Materials and Methods
Supporting Text
Figs. S1-S14
References

Supporting On-line Material

Feng Tao,[1,2] Sefa Dag,[3] Lin-Wang Wang,[3] Zhi Liu, [4] Derek R. Butcher,[1,2] Hendrik Bluhm,[5] Miquel Salmeron,[2]* Gabor A. Somorjai [1,2]*

Materials Science Division, Lawrence Berkeley National Lab, Berkeley CA 94720 [1]
Department of Chemistry, University of California, Berkeley CA 94720 [2]
National Energy Research Scientific Computing Center, Lawrence Berkeley National Lab, Berkeley CA 94720 [3]
Advanced Light Source, Lawrence Berkeley National Lab, Berkeley CA 94720 [4]
Chemical Science Division, Lawrence Berkeley National Lab, Berkeley CA 94720[5]

1. In-situ Surface Analytical Techniques Operated under Ambient and High Pressure Conditions

(a) Ambient Pressure XPS (APXPS)

A photoelectron spectrometer capable of operating under ambient pressures (up to a few Torr) was developed at the Lawrence Berkeley National Laboratory (*S1-4*). To overcome the short mean free path (λ) of the photoelectrons traveling through a gas phase (a few mm in the hundreds of Pascal range), the sample is located close to the small aperture of a cone (∅<0.3 mm) at a distance < λ (Fig. S1). This aperture separates the ambient pressure environment of the reactor from a first pumping stage. This is followed by three other differentially pumped stages with the apertures that separate them located at the focal plane of an electron optics system that focuses the electrons into a hemispherical analyzer located in the final chamber (Fig. S1a). The instrument takes advantage of the variable energy of synchrotron generated X-rays to obtain non-destructive depth profiles of composition and chemical state near the surface by virtue of the varying mean free paths of electrons inside the material.

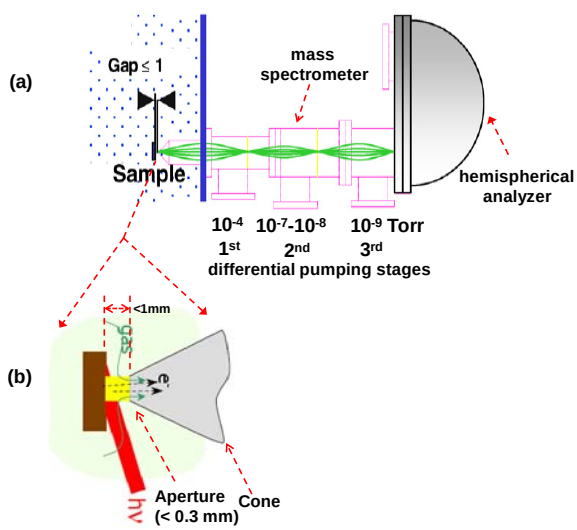

Fig. S1. Schematic diagrams of the ambient pressure XPS. A cone aperture (b) is used to separate the high pressure environment of sample from high vacuum environment required for the energy analyzer.

(b) High Pressure STM

Scanning tunneling microscope (STM) has the unique capability of imaging surfaces with atomic resolution. The technique can be applied in a pressure range from UHV to atmospheric and even higher pressures, since the tunneling process between the sample and tip only occurs in a very close range of 5–50 Å. In previous studies a large volume (a few liters or much larger) STM chamber was connected to the UHV preparation chamber through a gate valve (*S5-8*). The new high pressure and high temperature STM used in the present study consists of a small cylinder reactor chamber with a volume of approximately 19 cm^3. The reactor is mounted inside the vacuum environment of the UHV chamber using a special docking scaffold (Fig. S2a). It is vibrationally isolated from the UHV chamber with springs, which greatly reduce vibrational noise and facilitate atomic resolution imaging (*S9*). Both the sample and tip can be conveniently placed and transferred using a transfer arm and wobble stick.

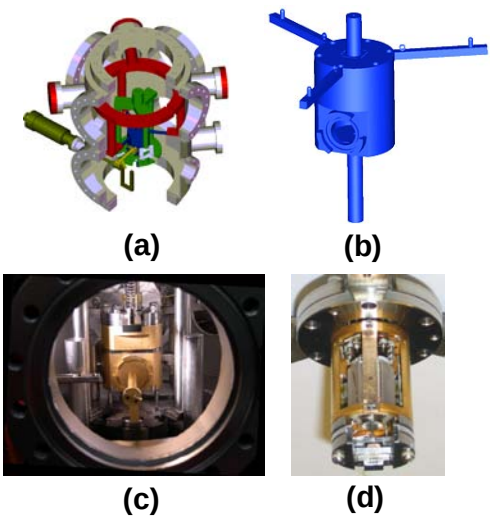

Fig. S2. (a) Schematic showing the design of chamber-in-chamber high pressure STM system. (b) Schematic of the small volume high pressure reactor showing the insertion gate (circular aperture) which allows sample transfer between the STM head and external sample preparation chamber. (c) Photo of high pressure reactor. (d) Photo of STM head with sample assembly stage.

2. Surface Structures and Preparation of Pt(557) and Pt(332)

The Pt(557) and Pt(332) single crystals were purchased from Metal Crystals & Oxides Ltd. Their orientation accuracy is <0.3°. Both of them have monoatomic steps and (111) oriented terraces 6 atoms wide. The atoms at the step edges of these crystals have (100) and (111) packing geometries, respectively, as shown schematically in Figure S3. The coordination number of the atoms on the upper side of the step edges is 7 for both Pt(557) and Pt(332). However, the coordination number of the atoms on the lower step side (Figs. S3c and S3d) is 10 and 11 for Pt(557) and Pt(332), respectively.

Clean Pt(557) and Pt(332) were prepared by Ar ion sputtering and by annealing at 650-700°C in a pressure of oxygen of ~5×10^{-8} Torr. This was followed by annealing to 800°C in UHV. The cleanness of the surfaces was checked with XPS and STM before reaction studies.

Ultrapure carbon monoxide (99.999%) was used as source of reactant gas. A trap containing copper granules (99.990%, Aldrich Ltd) was used to dissociate any possible metallic carbonyl impurity formed in the gas cylinder and delivering system.

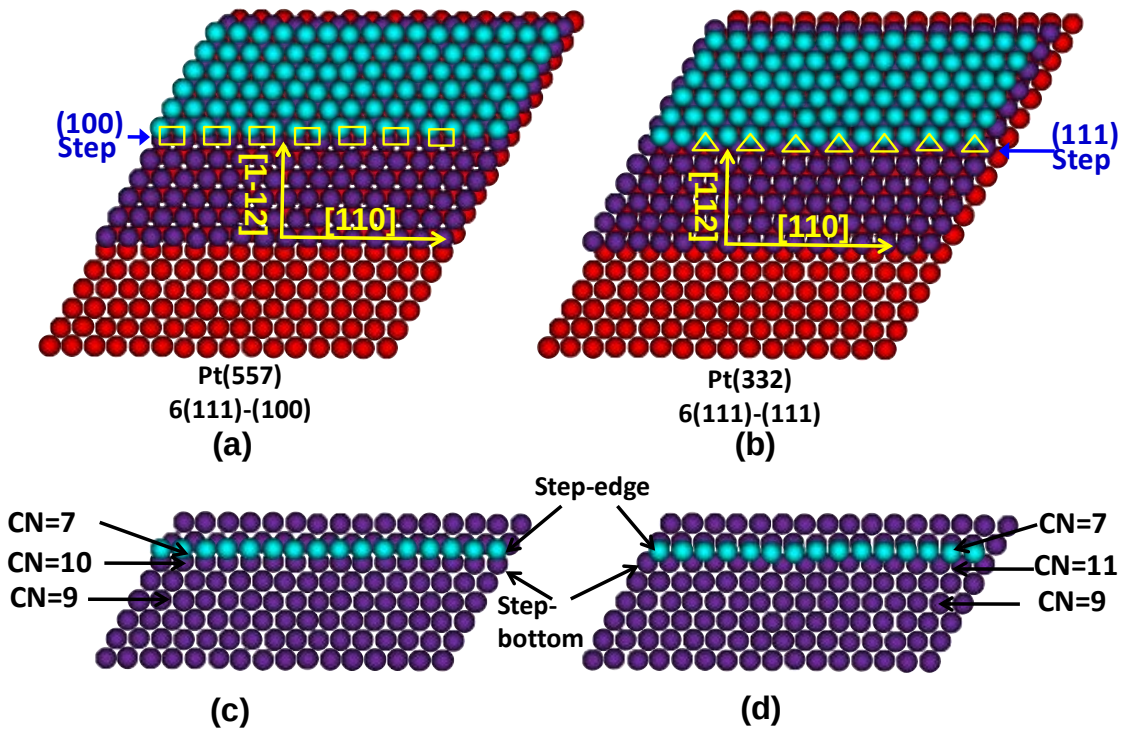

Fig. S3. Schematics of Pt(557) (a) and Pt(332) (b) surfaces. (c) and (d): Geometry and coordination numbers of Pt atoms at (100) step of Pf(557) and (111) step of Pt(332).

3. Data Analysis and Deconvolution

Photoemission of electrons from the Pt4f, O1s, and C1s core levels were produced with X-rays with energies of 340, 800, and 560 eV, respectively. This choice of photon energies ensured similar kinetic energy of the emitted photoelectrons and thus equal depth of analysis. Valence band spectra were also collected under the same experimental conditions. The binding energy in each spectrum was calibrated by the Fermi level of the valence band spectra collected under the same experimental conditions. The shapes of the XPS peaks were deconvoluted into component peaks of fixed energy, width, and shape.

4. STM Images of Pt(557) under CO Environments with Different Pressures

Fig. S4 shows four representative STM images of the Pt(557) surface under different conditions. They all have the same dimensions of 40 nm × 50 nm. Fig. S4a is an image of the clean surface showing the steps and terrace structure running roughly along the diagonal from bottom left to upper right. The measured width of each terrace is ~12 Å. After the clean surface was exposed to CO gas at a pressure of ~5×10^{-8} Torr, terraces with different widths were observed, with an average value of ~ 26 Å, which indicates a doubling of the terrace width. Line-profile analysis indicates that these terraces are separated by steps ~4.0-4.5 Å high. An important observation is the step structure which has changed from nearly straight to meandering at this pressure. Fig. S5 shows schematically the surface structure of the clean Pt(557) consisting of terraces with single-atom height steps (a), and surfaces consisting of double terraces with double-atom height steps.

After further increasing the pressure to ~1 Torr, the surface became covered with nanoclusters with an average size of about 2.2 nm × 2.1 nm along [112] and [1-10] directions, respectively (Fig. S4d). The clusters have a roughly triangular shape.

5. STM Images of Pt(332) Obtained at High Pressure and Low Pressure

Fig. S6 presents two STM images of Pt(332) under CO pressure of 2×10^{-8} Torr (a) and 1 Torr (b). In contrast with the Pt(557) surface, the steps retain their straight alignment when covered by CO at low pressure (left image). Like the Pt(557), under high CO pressure (>0.1Torr) the surface breaks up into nanoclusters. However, instead of the triangular shapes formed on Pt(557), on Pt(332) the nanoclusters are rectangular or roughly parallelogram in shape, as shown in Fig. S6b.

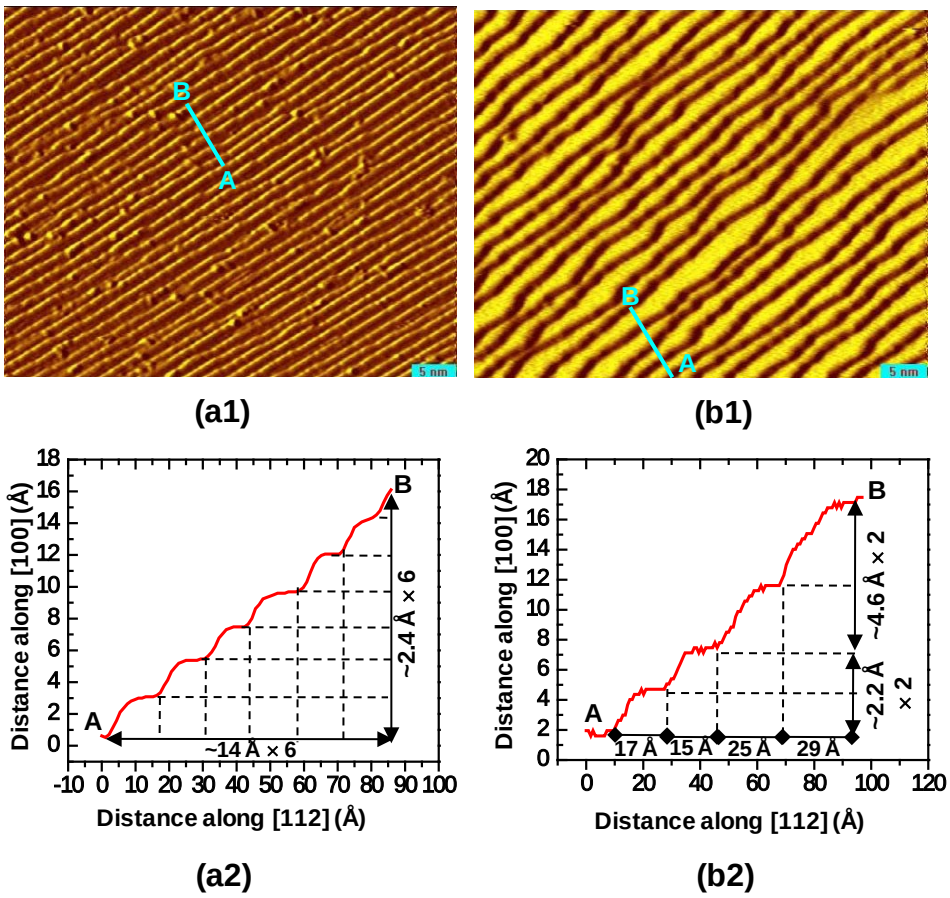

Fig. S4. STM images and line-profiles of the Pt(557) surface in different conditions. (a1) Clean surface in a background pressure of 1×10^{-10} Torr. (a2) Line-profile along A-B in (a1). (b1) Pt(557) under 5×10^{-8} Torr of CO. (b2) Line-profile along A-B in (b1). (c1) Surface structure of Pt(557) after increasing the CO pressure to 5×10^{-7} Torr. (d1) Surface structure of Pt(557) after increasing the CO pressure to 1 Torr.

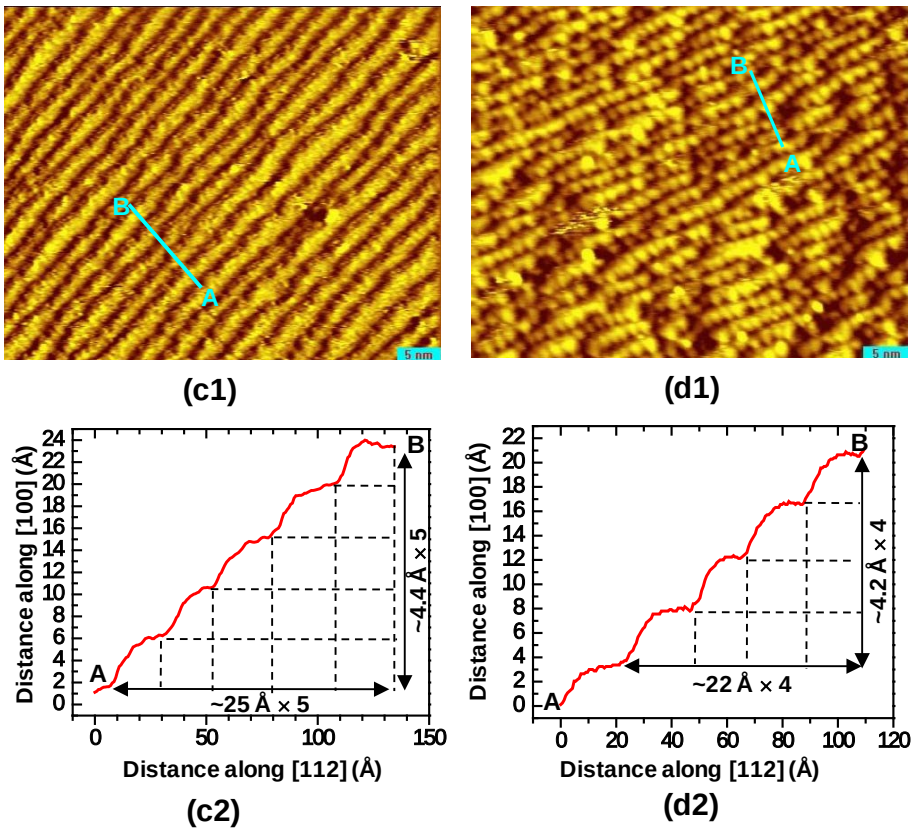

Fig. S4. (**Continued**) STM images and line-profiles of the Pt(557) surface in different conditions. (a1) Clean surface in a background pressure of 1×10^{-10} Torr. (a2) Line-profile along A-B in (a1). (b1) Pt(557) under 5×10^{-8} Torr of CO. (b2) Line-profile along A-B in (b1). (c1) Surface structure of Pt(557) after increasing the CO pressure to 5×10^{-7} Torr. (b2) Line-profile along A-B in (b1). (d1) Surface structure of Pt(557) after increasing the CO pressure to 1 Torr.

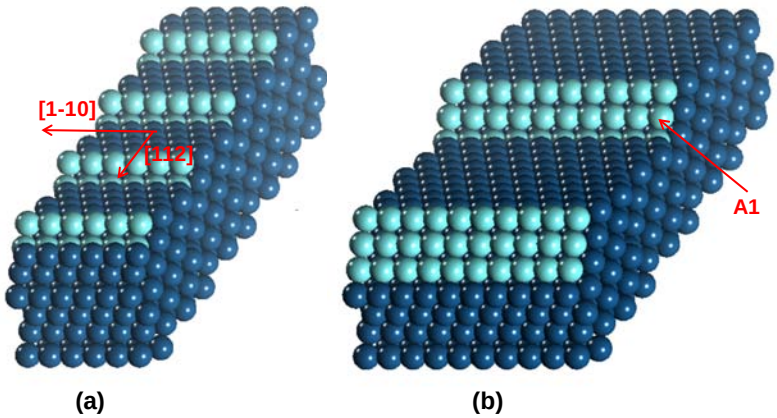

Fig. S5 (a) Schematic of clean Pt(557) consisting of terraces with single-atom height; (b) schematic of clean Pt(557) consisting of double-atom height.

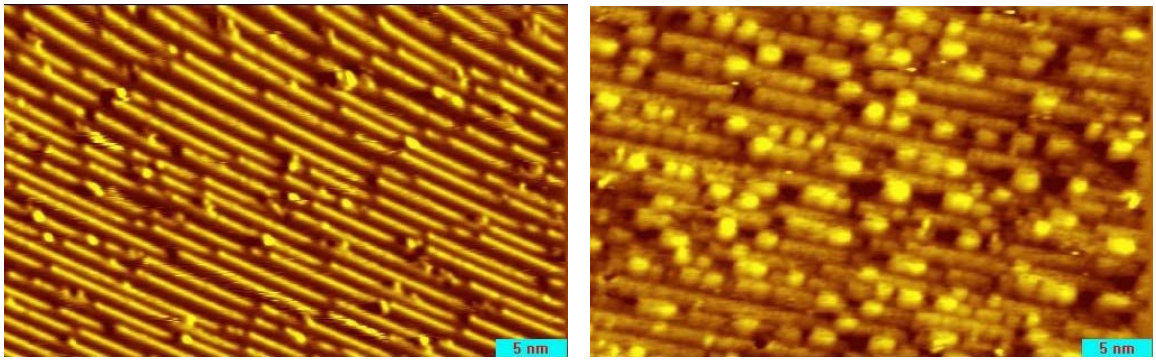

(a) (b)

Fig. S6. (a) STM image of the Pt(332) surface in a CO environment with pressure of 2×10^{-8} Torr; (b) STM image of Pt(332) in a CO environment with a pressure of 1 Torr. The size of both images is 25 nm × 40 nm. The surface has broken up into clusters of rectangular shapes.

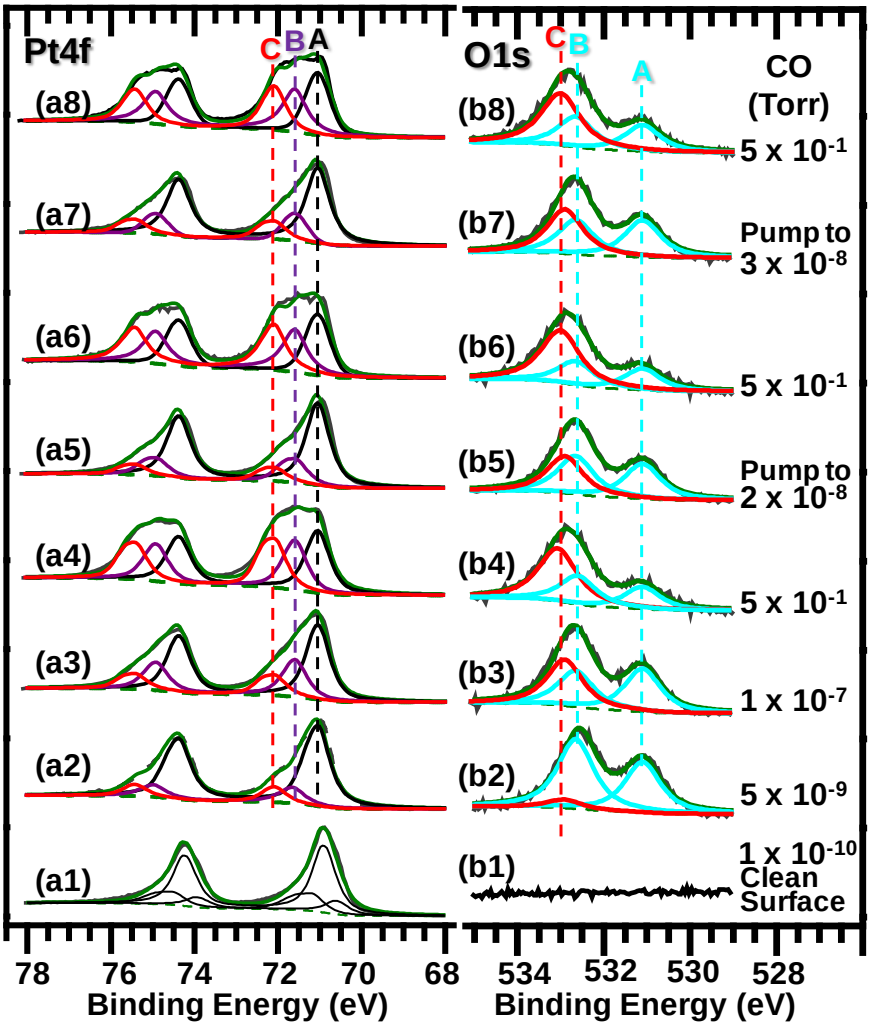

Fig. S7. Deconvoluted Pt4f and O1s spectra of Pt(557) in CO under different reaction conditions.

6. Analysis of the Photoemission Features of Pt4f and O1s on Pt(557)

Fig. S7 presents the photoemission features of Pt4f and O1s collected under a sequence of reaction conditions. On the basis of published deconvolution parameters for Pt(557) (*S10*), the Pt4f spectrum of the clean surface was deconvoluted into three peaks at 71.05 eV for bulk, 70.75eV for terrace, and 70.40 for step atoms respectively. After CO adsorption the deconvolution was performed using published XPS data of CO adsorption on Pt(311) (=3(111)-(111)) *(S10)* at low pressure (10^{-9} to 10^{-8} Torr). The Pt $4f_{7/2}$ spectrum consists now of three peaks assigned to bulk Pt (peak A), Pt atoms bound with CO in top and bridge positions (peak B), and under-coordinated Pt atoms bound with CO (peak C). The positions and widths of the peaks were fixed at 71.10 and 0.68 eV (peak A), 71.70 and 0.68 eV (peak B), and 72.15 eV and 0.68 eV (peak C) for all reaction conditions.

On the basis of published data (*S11, 12*), the bindng energy O1s from CO bonded on on-top and bridge sites of Pt(111) and Pt(335) are 531.0 and 532.6 eV, respectively. Similarly, the O1s photoemission spectra were also deconvoluted into three peaks (A, B, and C), corresponding to CO molecules bound to Pt on bridge sites (peak A), on-top sites (peak B), and under-coordinated Pt atoms (peak C). The positions of peaks A and B were fixed at 531.0 and 532.6 eV and widths at 1 eV, following published data for CO on Pt(355) at low pressure (*S11*). Two methods were used to constrain position and width of peak C. In the first the position and width of peak C were fixed at 533.1 eV and 1.0 eV for spectra at 5×10^{-1} Torr (Figs. S7b4, S7b6, and S7b8), and 532.95 eV and 1.0 eV for spectra at low pressure (Figs. S7b2, S7b3, S7b5, and S7b7), since the O1s peak high binding energy tail obtained at high pressure (5×10^{-1} Torr) shifts to higher energy, in contrast to those collected at low pressures. In the second method the positions and widths of all C peaks at both high pressure and low pressure were fixed at 532.95 eV and 1.0 eV. The second method gave a slightly higher fraction for the area of peak C for the spectra obtained at high pressures, but otherwise the results were quite similar. As the standard deviation of the deconvoluted spectra obtained with the first method is slightly lower than that obtained with the second method, Fig. S7 were obtained with the first method. This deconvolution is reasonable. For example, at 5×10^{-9} Torr about 52% and 38% of the adsorbed CO molecules are bound to atop and bridge sites respectively, and only ~10% are bound to under-coordinated Pt atoms, which is well consistent with the fraction of CO on different sites on Pt(322) (=5(111)-(100) with c(2×4) adsorbate layer (*S11*).

Fig. 4 shows the coverage of CO molecules bound to under-coordinated Pt sites for several reaction conditions. For example, at 5×10^{-1} Torr ~57% of the CO molecules are bound to under-coordinated Pt atoms. In fact, for an equilateral triangular nanocluster proposed by DFT calculations, the ratio of edge Pt atoms to the total surface Pt atoms is ~52% (back triangular frame in Fig. 3c). It is basically consistent with the measured coverage of CO molecules bound to under-coordinated Pt atoms deduced from the XPS peak areas, though the observed shape of triangular nanoclusters is not equilateral. After CO was pumped to 2×10^{-8} Torr, the fraction of Pt atoms at cluster edge bound to CO molecules is decreased to ~20%, which is consistent with the recovery of a flat terrace with meandering steps as visualized by STM. This alternating increase and decrease of the fractions of under-coordinated Pt atoms at step/cluster edge in a few cycles of high pressure and low pressure indicates that the observed restructuring is reversible.

7. STM imaging of Pt(557) following High Pressure–Low Pressure CO Exposure Cycles

Figs. S8a and S8b show images obtained at 1 Torr CO pressure and after pumping down to 10^{-8} Torr. The nanoclusters in Fig. S8a have an average size close to that of Fig. S4d1. Fig. S8b shows a kink decorated step surface formed after the CO gas phase was pumped down. The average width of terraces and height of step is ~ 24 Å and ~4.4 Å. The structure of the surface after pumping the CO (Fig. S8b) is very similar to that obtained by directly exposing the clean

Pt(557) to CO at a pressure of 5×10^{-8} Torr (Fig. S4b). After a few cycles of filling the reactor cell to CO at ~1 Torr followed by pumping to 10^{-8} Torr, the surface morphology became rougher.

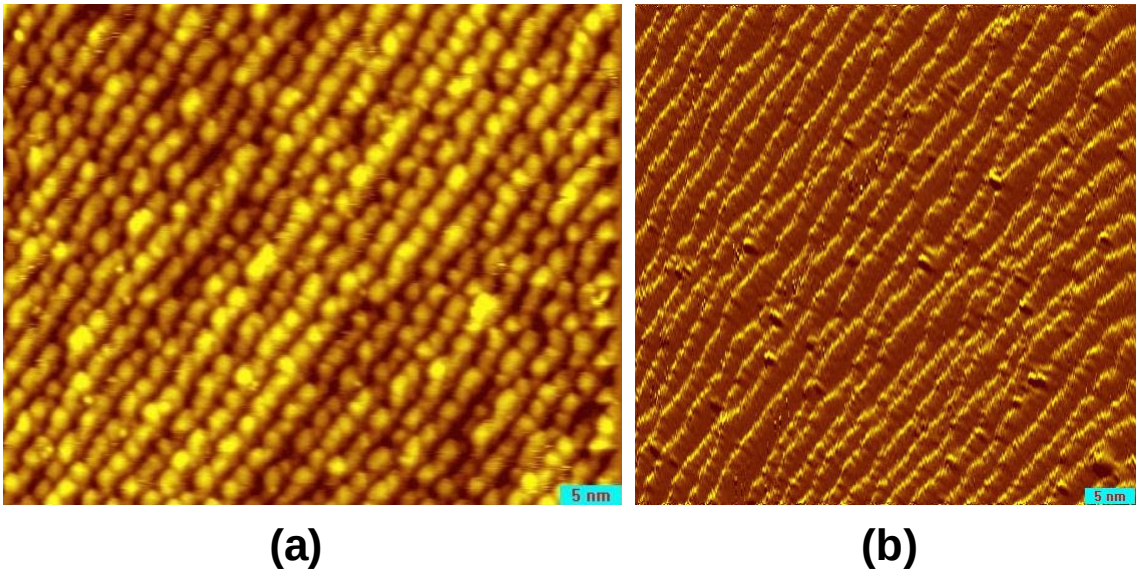

Fig. S8. STM images of Pt(557) after a sequence of reactions cycling between high and low pressure. (a) In 1 Torr of CO; (b) After the CO gas was pumped to ~10^{-8} Torr.

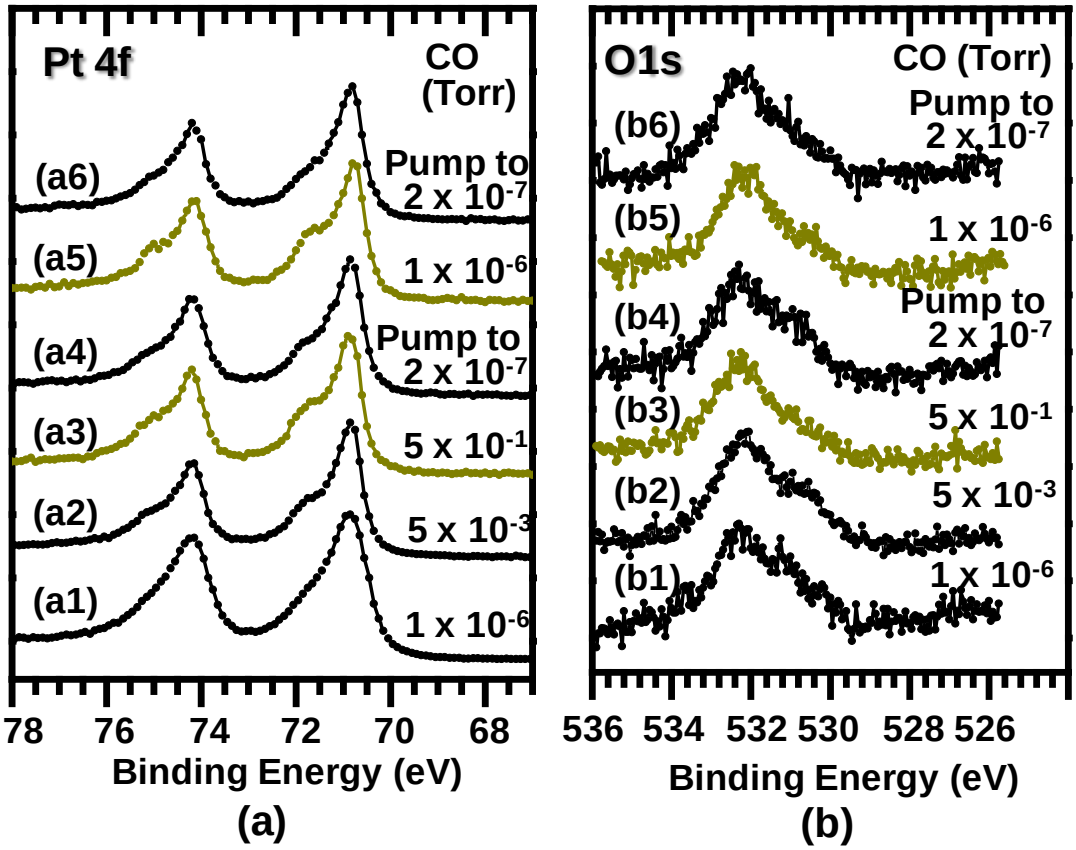

Fig. S9. Pt4f an O1s spectra of Pt(111) under different CO environments.

8. CO Coverage on Pt(557) under Various Reaction Conditions

Fig. 2c shows the CO coverages on Pt(557) under different reaction conditions. The coverage of CO on Pt(557) under a CO pressure of 5×10^{-9} Torr was set to 0.5 on the basis of the known coverage of the c(2×4) on Pt(111) (*S13*) and Pt(322) and Pt(355) (*S14, 15*). The coverage of CO at other pressures was calculated by comparing the area ratio between the O1s peak and Pt4f to that at 5×10^{-9} Torr.

At shown in Fig, 2c, at 10^{-7} Torr the coverage increased to 0.65. At 5×10^{-1} Torr the coverage increased further to 0.97, much higher than the value of ~0.65 on Pt(111) at the same pressure (*S13*). This difference is supported by the distinctly different photoemission features of Pt4f and O1s under similar pressures (Fig. 2a and 2b for Pt(557) versus Figs. S9a and S9b for Pt(111)).

Figs. 2 and S7 presents the photoemission features of Pt4f and O1s of Pt(557) under different CO pressures. As the pressure increases a shoulder in the high energy side of the Pt4f spectrum becomes identifiable and is predominant at 5×10^{-1} Torr. These changes can be assigned to the increased density of under-coordinated Pt atoms (step and kink sites and edges of nanoclusters). However, there is no such a significant contribution at high binding energy side in Pt4f spectra of Pt(111) (Fig. S9a3). There is no significant change in the O1s photoemission features after the CO pressure was increased to 5×10^{-1} Torr for Pt(111) (Fig. S9b). Since Pt(111) does not form nanoclusters at 5×10^{-1} Torr (*S13*), the photoemission feature of Pt4f at high binding energy sides observed at high pressure on Pt(557) can be assigned to the under-coordinated Pt atoms forming the edges of the nanoclusters.

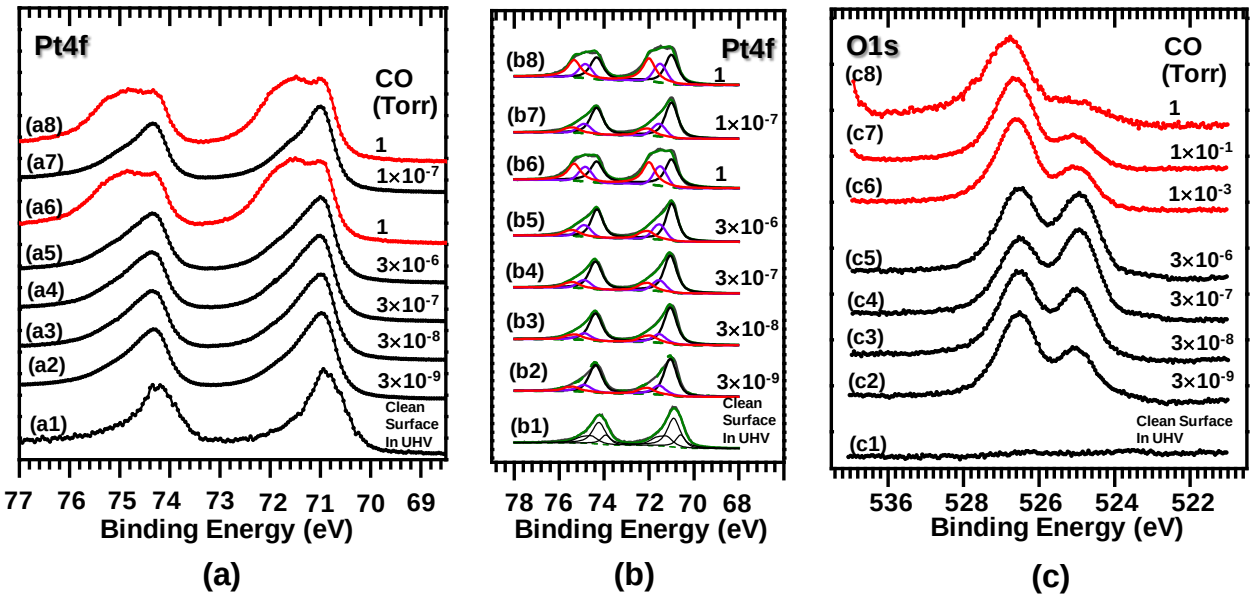

Fig. S10. (a) Pt4f spectra of Pt(332) under various pressures of CO; (b) Deconvoluted Pt4f spectra with the same fitting parameters used for the Pt4f peak of Pt(557); (c) O1s spectra of Pt(332) in a CO environment under different reaction conditions.

9. Ambient-Pressure XPS Studies of CO on Pt(332) at Different Pressures

Fig. S10a shows Pt4f spectra obtained on Pt(332) under different reaction conditions. Clearly, at high pressure (1 Torr), a significant contribution in the high binding energy sides can

be identified (Fig. S10a6). Corresponding to this new photoemission feature, a new contribution in the high binding energy side of O1s appears in Fig. S10c8. Fig. S10b presents the deconvolution of Pt4f spectra with the same parameters used for Pt(557). The alternating increase and decrease of the fraction of Pt 4f photoemission intensity at ~72.0 eV (Fig. S10b) shows the reversibility of nanocluster formation.

Fig. S11 presents the fractions of CO molecules bound to under-coordinated Pt sites of Pt(332) at different reaction conditions. Fig. S12 presents the CO coverage on Pt(332) at different pressures calculated by following a similar procedure as in the case of Pt(557). Similarly a large coverage of ~0.90 was reached at a pressure of ~ 1 Torr.

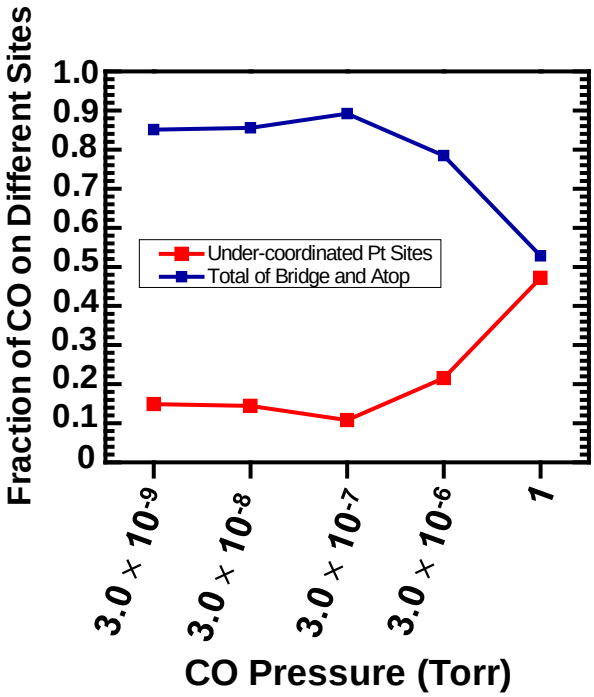

Fig. S11. Fraction of CO molecules bound to under-coordinated Pt atoms of Pt(332) and total fraction of CO molecules on top and bridge binding sites at different pressures.

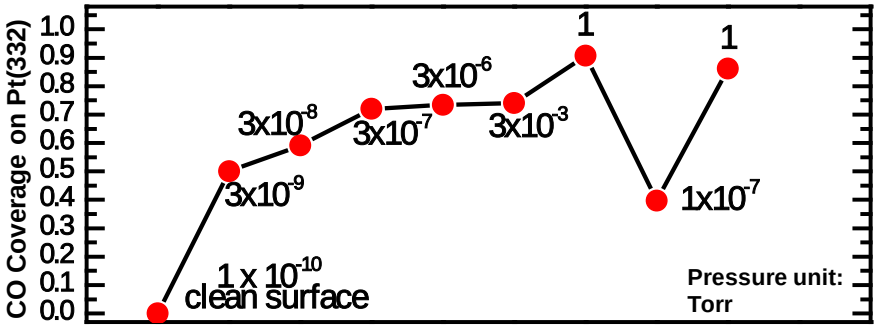

Fig. S12. Total CO coverage on Pt(332) at different pressures.

10. Computational Methods

All calculations presented in this paper were performed using the Vienna *ab initio* simulation package (VASP) [*S16-18*] at the National Energy Research Scientific Computing Center (NERSC) of the Lawrence Berkeley National Laboratory. First-principles total energy and electronic structure calculations were performed using the projector-augmented-wave (PAW) method [*S19-21*] within the local density approximation (LDA) [*S22*]. Energy cut-off for plane waves up to 400 eV and a Monkhorst-Pack [*S23*] k-point sampling with 5×3×1 k-point meshes for each Pt(557) and Pt(332) unit cell were used. Atomic relaxations were performed with the conjugate gradient method and relaxation was continued until the atomic forces were less than 0.01 eV/Å. The bulk crystal structure of Pt was relaxed with LDA and the lattice constant for fcc Pt bulk was found to be 3.924 Å, which is close to experimental lattice constant of 3.920 Å. Our terrace surface model contains 5 Pt layers and a vacuum buffer layer of 15 Å inside a periodic supercell. The system is periodic along the terrace and in-plane perpendicular directions. To mimic the semi-infinite crystal, the positions of atoms in the bottom 3 layers were kept fixed, while the atoms in the top two layers were allowed to relax during optimization.

11. Calculation Results for Surfaces with Half Monolayer CO Coverage

We built starting geometries for the various Pt stepped surfaces to be used in our calculations. At low pressure we prepared two surfaces with c(2×4) structures, one with single-atom step height, the other with two-atom step height and double terrace widths. These are denoted as Pt(557)-S-c(2×4) and Pt(557)-D-c(2×4) respectively. There are several possible structures corresponding to different locations of the CO molecules. There is also the possibility that each Pt atom at the step edge will have one CO molecule (edge with full CO coverage at low pressure). We have tested all these possibilities. Since the different CO arrangements might have different number of Pt atoms and CO molecules, we have taken into account the chemical potentials of Pt and gas phase CO in order to compare the relative stability of the different systems. In comparing the single and double terrace structures, we have used two unit cells (in the terrace direction) of the single terrace structure, so the surface areas of these two structures are the same. We have taken special care of the surface structure of the bottom Pt layer in the supercell, so that it is the same for single and double terraces. As a result, the relative stabilities of the single and double terraces can be judged based on their total free energies.

In contrast, the bottom layers of the Pt(557) and Pt(332) supercells cannot be made the same, thus they should not be compared directly. The minimum energy c(2×4) coverage configurations for different terraces are shown in Table S1. We found that the edge with full CO coverage is unstable. The minimum total free energy for different systems with the same surface area is defined as: $E_{free}(N_{Pt}, N_{CO}) = E_{unit\text{-}cell}+\Delta N_{Pt}\cdot E_{Pt}+\Delta N_{CO}\cdot E_{CO}$ and listed in the last column of Table S1. Here N_{Pt} and N_{CO} are the numbers of Pt atom and CO molecules in the system (shown in the 3rd and 4th columns), $E_{unit\text{-}cell}$ is the calculated energy of the unit cell (shown as the 5th column in Table S1), ΔN_{Pt} is the Pt number difference between the calculated unit cell and the N_{Pt} shown in the 6th column, ΔN_{CO} is the difference in the number of CO molecules. E_{Pt} = -7.4520 eV is the bulk Pt chemical potential, and E_{CO} is the CO molecule chemical potential. For the c(2×4) coverage, we have chosen E_{CO} = (-15.556-2.470) eV, where -15.556 eV is the calculated isolated CO energy, and -2.470 eV is the calculated average binding energy of CO on flat Pt (111) surface with a c(2×4) pattern. Thus E_{CO} is the CO chemical potential at the CO pressure when the c(2×4) coverage is formed.

Table S1. Free energies of unit cells and calculation slabs.

Entry	Step	Unit-Cell N_{Pt}	Unit-Cell N_{CO}	Unit-Cell Energy (eV)	Free Energy with N_{Pt}= 204 (eV)	Relative Free Energy (eV)
1	Pt(557)-S-CS	204	0	-1477.274	-1477.274 (N_{CO}=0)	0
2	Pt(557)-D-CS	194	0	-1402.506	-1477.026 (N_{CO}=0)	-0.248 (taking Entry #1 as reference)
3	Pt(332)-S-CS	192	0	-1389.721	-1479.144 (N_{CO}=0)	0
4	Pt(332)-D-CS	182	0	-1314.854	-1478.797 (N_{CO}=0)	+0.348 (taking Entry #3 as reference)
5	Pt(557)-S-c(2×4)	204	10	-1656.270	-1674.296 (N_{CO}=11)	0
6	Pt(557)-D-c(2×4)	194	11	-1600.568	-1675.088 (N_{CO}=11)	-0.7128 (taking Entry #5 as reference)
7	Pt(332)-S-c(2×4)	192	10	-1568.950	-1676.400 (N_{CO}=11)	0
8	Pt(332)-D-c(2×4)	182	10	-1494.397	-1676.366 (N_{CO}=11)	+0.034 (taking Entry #7 as reference)

S: Single steps; D: Double steps. CS: Clean surface.

From Table S1, the clean double terraces for both Pt(557) and Pt(332) have higher energy than the clean single terraces of these surfaces, which means the terrace will not transit from single to double terrace without CO adsorption. But this energy is small, in the order of 0.1 to 0.2 eV per edge atom. They are probably also in the accuracy limit of the DFT calculations. Notably, the energy of Pt(332)-S-CS (entry 1 in Table S1) is 1.870 eV lower than that of Pt(557)-S-CS. Thus, we can conclude that the Pt(332)-S-CS terraces are more stable than the Pt(557)-S-CS terraces. This is because the Pt(332)-S-CS has (111) steps, whereas Pt(557) has (100) steps.

With the c(2×4) CO coverage, the Pt(557) double terrace has lower free energy than its single terrace counterpart (entry 5 and 6 in Table S1). Thus, the double terrace becomes more stable, consistent with the experiments. Note that the listed free energy for Pt(557)-S-c(2×4) in Table S1 is likely underestimated since the chemical potential E_{CO} used was estimated at a very low pressure. At the experimental pressure, the E_{CO} will be higher, thus the free chemical potential of Pt(557)-S-c(2×4) will be even larger, which makes it more unfavorable compared

with Pt(557)-D-c(2×4). On the other hand, for the Pt(332) surface the double terrace with adsorbed CO (c(2×4), entry 8 in Table S1) is still slightly higher in energy than the single terrace under c(2×4) CO coverage (entry 7 in Table S1), though the difference is very small. As a result, the doubling step transition for Pt(332) upon CO adsorption at low pressure is not energetically favorable, in agreement with the experimental observations.

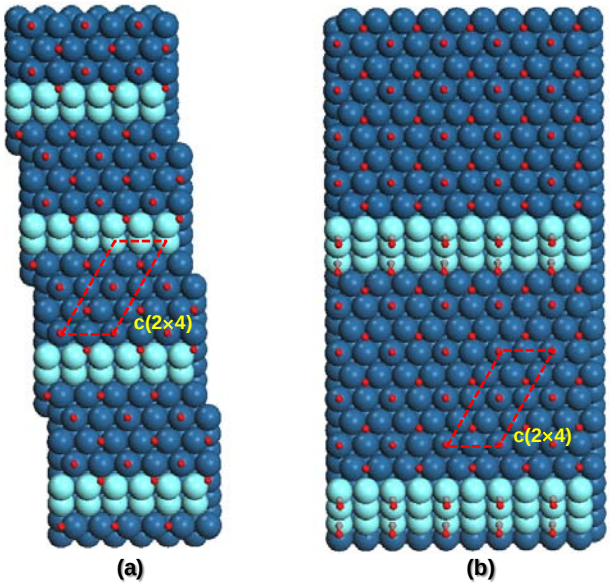

Fig. S13. (a) Optimized DFT structure of Pt(557) consisting of terraces with single-atom steps and adsorbed CO molecules forming a c(2×4) pattern; (b) Optimized structure of Pt(557) consisting of terraces with double-atom step heights and CO molecules forming a c(2×4) structure.

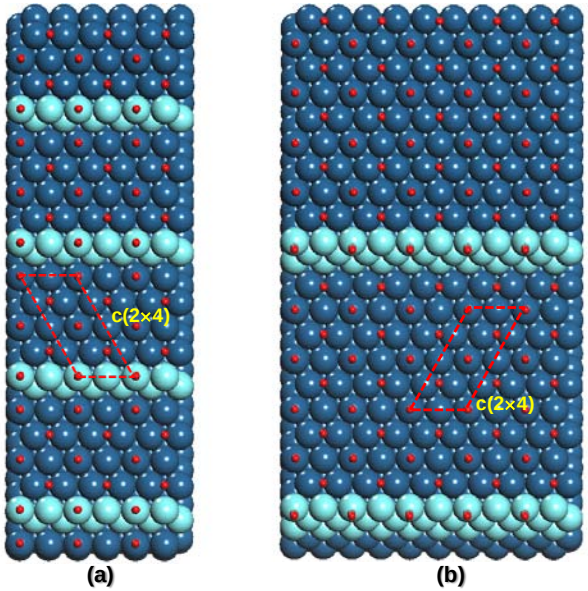

Fig. S14. (a) Optimized structure of Pt(332) consisting of terraces with single-atom steps covered by adsorbed CO molecules with c(2×4) pattern; (b) Optimized structure of Pt(332) consisting of terraces with double-atom steps and adsorbed CO molecules with c(2×4) structure.

12. Calculation Results for Pt(557) Double Terrace under (1×1) CO Coverage

The shape of nanoclusters observed in the STM images is that of a triangle pointing outward to the terrace, although some times, depending on tip sharpness, molecular mobility, and image resolution, the shape is not as well resolved. To simplify the calculation, we built models with equilateral triangular clusters as starting geometries, although the experimental nanoclusters need not be exactly equilateral. Three slabs with different potential structures fully covered with CO molecules were built. The first is a double terrace with a CO coverage of 1 (Fig. 3a). The second is a double terrace with a parallelogram nanocluster created by removing two Pt rows (Fig. 3b), a model that serves to test the shape effects on the total energy. The third is a double terrace with a one atomic layer high triangular cluster (Fig. 3c). The numbers of Pt atoms on surfaces of these structures are also the same and the numbers of adsorbed CO molecules on them are the same. Thus their energies, listed in Table S2, can be compared directly.

To evaluate the influence of the thickness of the slab on the adsorption energy of CO, calculations with slabs of only three layers of Pt atoms were performed as well. We found that the difference in adsorption energy is less than 40 meV per atom or CO molecule. In some cases whether or not a surface Pt should be bound to a CO molecule cannot be decided by physical intuition. One example is the row of Pt atoms immediately at the bottom of the two layer height step edge. In that case, the CO gas chemical potential is used to estimate whether to occupy those sites. The CO chemical potential for (1×1) coverage is calculated as: $\mu_{CO} = E_{CO}(isolated) + E_{CO}(binding,111) + kT\ln(P/P_0)$, here E_{CO}(isolated)= -15.556 eV is the isolated CO energy calculated by LDA, E_{CO}(binding,111) is the binding energy of CO on a Pt(111) surface with 1×1 coverage, which is -1.695 eV as calculated by LDA. P_0 is gas pressure, at which the coverage on (111) terrace is changed from half monolayer of c(2×4) coverage to (1×1) coverage, and P is the actual experimental CO pressure. At a pressure of 5×10^{-1} Torr, $P/P_0 \approx 100$, and thus the entropy contribution to the CO chemical potential is about 0.11 eV. Using this CO chemical potential, we found that covering the Pt atoms at the bottom of the steps of a double-layer (100) step gives a lower energy by 0.132 eV per CO molecule. So, we decided to cover that row. The total energies for these three systems are listed in Table S2.

Table S2. Free energies of three potential structures under (1×1) CO coverage.

Entry	Terrace with 1×1 CO coverage	Unit-Cell N_{Pt}	Unit-Cell N_{CO}	Free Energy with N_{Pt}=340 N_{CO}=110	Free Energy with N_{Pt}=340 N_{CO}=110
1	Pt(557) regular (D terrace))	340	110	0 (set as energy reference)	-4233.234
2	Pt(557) parallelogram (D terrace)	320	99	-23.432 (taking Entry #1 as reference)	-4257.666
3	Pt(557) triangle (D terrace)	295	100	-10.445 (taking Entry #1 as reference)	-4243.679

The calculated total free energies listed in Table S2 show that triangle shape is the most stable structure, followed by the parallelogram structure, then the flat terrace with double-atom high steps.

References

1. D. F. Ogletree , H. Bluhm , G. Lebedev , C. S. Fadley , Z. Hussain , M. Salmeron , *Rev. Sci. Instrum.* **73**, 3872 (2002).
2. Salmeron, M; Schlogl, R, *Surf. Sci. Rep.* **63**, 169 (2008).
3. H. Bluhm, M. Havecker , A. Knop-Gericke, M. Kiskinova, R. Schlogl, M. *MRS Bull.* **32**, 10222 (2007).
4. F. Tao, M. E. Grass, Y. Zhang, D. R. Butcher, J. R. Renzas, J. Y. Chung, Z. Liu, S. B. Mun, M. Salmeron, G. A. Somorjai, *Science* **322**, 932 (2008).
5. K. B. Rider, K. S. Hwang, M. Salmeron, G. A. Somorjai, *J. Am. Chem. Soc.* **124**, 5588 (2002).
6. M. Montano, K. Bratlie, M. Salmeron, G. A. Somorjai, *J. Am. Chem. Soc.* **128**, 13229 (2006).
7. B. J. Mcintyre, M. Salmeron, G. A. Somorjai, *Science* **205**, 1415 (1994).
8. B. J. Mcintyre, M. B. Salmeron, G. A. Somorjai, *Catal. Lett.* **14**, 263 (1992).
9. F. Tao, D. Tang, M. Salmeron, G. A. Somorjai, *Rev. Sci. Instrum.* **79**, 084101 (2008).
10. A. Apai, R. C. Baetzold, P. J. Jupiter, A. J. Viescas, I. Lindau, *Surf. Sci.* **134**, 122 (1983).
11. O. Bjornebolm, A. Nilsson, H. Tillorg, P. Bennich, A. Sandell, B. Hernnas, C. Puglia, N. Martensson, *Surf. Sci.* **315**, L983 (1994).
12. M. Kinne, T. Fuhrmann, C. M. Whelan, J. F. Zhu, J. Pantfo¨ rder, M. Probst, G. Held, R. Denecke, H.-P. Steinru¨ck, *J. Chem. Phys.* **117**, 10852 (2002).
13. S. R. Longwitz, J. Schnadt, E. K. Vestergaard, R. T. Vang, E. Lægsgaard, I. Stensgaard, H. Brune, F. Besenbacher, *J. Phys. Chem. B* **108**, 14497 (2008).
14. B. Tränkenschuh, N. Fritsche, T. Fuhrmann, C. Papp, J. F. Zhu, R. Denecke, H.-P. Steinrück *J. Chem. Phys.* **124**, 074712 (2006).
15. B. Trankenschuh, C. Papp, T. Fuhrmann, R. Denecke, H.-P. Steinruck, *Surf. Sci.* **601**, 1108 (2007).
16. G. Kresse and J. Hafner, *Phys. Rev. B* **47**, 558 (1993).
17. G.Kresse and J. Furthmuller, *Comput. Mater. Sci.* **6**, 15 (1996).
18. G. Kresse and J. Furthmuller, *Phys. Rev. B* **54**, 11169 (1996).
19. M.C. Payne, M. P. Teter, D. C. Allen, T. A. Arias, and J. D. Joannopoulos, *Rev. Mod. Phys.* **64**, 1045 (1992).
20. P. E. Blochl, *Phys. Rev. B* **50**, 17953 (1994).
21. G. Kresse, D. Joubert, *Phys. Rev. B* **59**, 1758 (1999).
22. J. P. Perdew, A. Zunger, *Phys. Rev. B* **23**, 5048 (1981).
23. H. J. Monkhorst and J. D. Pack, *Phys. Rev. B* **13**, 5188 (1976).